

In-situ formed and low-temperature deposited Nb: TiO₂ compact-mesoporous layer for hysteresis-less perovskite solar cells with high performance

Miao Yu

State Key Laboratory of Electronic Thin films and Integrated Devices, University of Electronic Science and Technology of China

Haoxuan Sun

State Key Laboratory of Electronic Thin Films and Integrated Devices, University of Electronic Science and Technology of China

Xiaona Huang

Chengdu Technological University

Yichao Yan (✉ yanyichao@uestc.edu.cn)

State Key Laboratory of Electronic Thin Films and Integrated Devices, University of Electronic Science and Technology of China <https://orcid.org/0000-0001-7889-6394>

Wanli Zhang

State Key Laboratory of Electronic Thin Films and Integrated Devices, University of Electronic Science and Technology of China

Nano Express

Keywords: perovskite solar cells, titanium oxide, low-temperature, hysteresis

Posted Date: May 26th, 2020

DOI: <https://doi.org/10.21203/rs.2.24741/v2>

License:   This work is licensed under a Creative Commons Attribution 4.0 International License.

[Read Full License](#)

Version of Record: A version of this preprint was published on June 22nd, 2020. See the published version at <https://doi.org/10.1186/s11671-020-03366-1>.

Abstract

Recently, reported perovskite solar cells (PSCs) with high power conversion efficiency (PCE) are mostly based on mesoporous structures containing mesoporous titanium oxide (TiO_2) which is the main factor to reduce the overall hysteresis. However, existing fabrication approaches for mesoporous TiO_2 generally require a high temperature annealing process. Moreover, there is still a long way to go for improvement in terms of increasing the electron conductivity and reducing the carrier recombination. Herein, a facile one-step, in situ and low-temperature method was developed to prepare an Nb: TiO_2 compact-mesoporous layer to serve as both scaffold and electron transport layer (ETL) in PSCs. The Nb: TiO_2 compact-mesoporous ETL based PSCs exhibit suppressed hysteresis, which is attributed to the synergistic effect of the large interface surface area caused by nano-pin morphology and the improved carrier transportation caused by Nb doping. Such a high-quality compact-mesoporous layer allows the PSC to achieve a remarkable PCE of 19.74%. This work promises an effective approach for creating hysteresis-less and high-efficiency PSCs based on compact-mesoporous structures with lower energy consumption and cost.

Introduction

Organic-inorganic hybrid perovskites have been attracting great interest as promising light-absorbing materials owing to their large absorption coefficients, high carrier mobility, and ease of fabrication^[1-5]. Perovskite-based solar cells, photodetectors, light-emitting diodes (LEDs), and even memory devices have been widely investigated and established^[6-8]. Since the year 2009, the power conversion efficiencies of perovskite solar cells (PSCs) have maintained rapid growth from 3.8% to over 25% under standard AM 1.5 illumination^[9-12]. PSCs are generally fabricated with a mesoporous or planar structure^[13-15]. To this day, the reported PSCs with high power conversion efficiency (PCE) are typically based on mesoporous structures containing an indispensable mesoporous metal oxide^[16]. Titanium oxide (TiO_2) has been commonly used as an electron transport layer and the typical mesoporous-type PSC presented by Seok has a structure of FTO/compact TiO_2 /mesoporous TiO_2 and perovskite composite layer/ perovskite upper layer/PTAA/Au^[17]. As is often reported in the literature, mesoporous TiO_2 contributes most to mesoporous-type PSC for reducing the overall hysteresis^[18]. However, the fabrication of a mesoporous TiO_2 layer often requires a high-temperature (>450°C) annealing treatment, leading to large energy consumption and limiting its application in flexible devices^[19-21]. Compared with the mesoporous-type PSCs, planar-type PSCs can be fabricated using a low temperature and low-cost processes^[22]. However, planar-type PSCs usually suffer from poor electron conductivity, severe charge recombination, and relatively lower crystallinity, resulting in low PCE with severe hysteresis behavior^[23-24].

Extensive efforts have been made to develop high-quality TiO_2 electron transport layers (ETLs) with high electron mobility, such as through morphology optimization, surface modifications, and doping. In particular, a wide range of elements have been chosen to prepare TiO_2 doping layers in PSCs, including

Indium (Li) [25-26], Niobium (Nb) [27-28], Platinum (Pt) [29], Sodium (Na) [30], Neodymium (Nd) [31], and Aluminum (Al) [32]. For instance, it is reported that the Li-doped TiO₂ is beneficial to the performance of the mesoporous-structure PSCs, especially the hysteresis effect [26]. Liao et al. reported a Pt-doped TiO₂ ETL which was demonstrated to improve the charge carrier extraction and injection efficiency in n-i-p PSCs [29]. Other ions such as Na, Nb and transition metal ions [30-31, 33-35] were used to modify surface or passivate defect of TiO₂, contributing to less non-radiative recombination. Among these elements, Niobium metal (Nb) is a good candidate as a doping material for titanium oxide electron transport materials due to its similar radius with that of titanium. The results shown by Yin et al. demonstrated that Nb doping can make an improvement in both conductivity and mobility, simultaneously decrease the trap-state density of TiO₂ ETLs for PSCs [27]. Despite this progress, a relatively high temperature (150 °C) treatment is mandatory and large hysteresis is still observed in PSCs based on Nb-doped TiO₂. As is well known, current density-voltage (*J-V*) hysteresis is a critical issue that occurs frequently, especially in planar-structure PSC devices. Severe hysteresis can lead to instability of PSCs and degradation of PCE. For this reason, it richly rewards the effort to develop a hysteresis-less PSC utilizing a simple and low-temperature method.

Here, we proposed a facile one-step, in situ and low-temperature (70°C) strategy to develop a hysteresis-less PSC, in which an Nb: TiO₂ compact-mesoporous layer served as both scaffold and ETL. The Nb: TiO₂ layer contained a compact TiO₂ layer with nano-pin morphology on the surface, which was utilized as a scaffold layer. The hysteresis index decreased significantly from 24.39% for the PSC based on bare TiO₂ to 3.19% for that based on 2% Nb: TiO₂ layer due to the collaborative effect of the large interface surface area caused by nano-pin morphology on the surface and the improved carrier transportation rate because of the presence of Nb. The high-quality mesoporous layer allowed the PSC to achieve a remarkable PCE of 19.7%. This work promises an effective approach for achieving hysteresis-less and high-efficiency PSCs through scalable and inexpensive methods at low temperature.

Methods

Sample Preparation

First, the FTO substrates were successively put into acetone, alcohol, and deionized water for ultrasonic cleaning for 30 minutes each. After that, the cleaned substrates were treated by a UV-ozone cleaner for 20 min and then placed in a petri dish. Second, 0.1 M TiCl₄ was dropped into deionized ice water mixture to prepare TiCl₄ aqueous solution. Third, 2% 0.1 M NbCl₅ was put into the ethanol near the temperature of 0 °C to obtain NbCl₅ ethanol solution. Then, the NbCl₅ ethanol solution and TiCl₄ aqueous solution were sequentially dropped into the petri dish containing FTO substrates. After hydrothermal reacting at 70°C for 60 min, the Nb: TiO₂ nano-pin features were formed on the FTO substrate.

The perovskite absorption layer was deposited with the dynamic two-step spin coating method [36]. First, the PbI₂ precursor solution was obtained by adding 0.462 g PbI₂ into 1 mL DMF. Meanwhile, the CH₃NH₃I

(MAI) precursor solution was obtained by adding 0.1 g MAI into 2 mL isopropanol (99.5%, Aladdin). Second, 55 μL PbI_2 precursor solution was spun onto the as-prepared Nb: TiO_2 ETL film at 3000 rpm for 10 s. At this moment, 55 μL MAI precursor solution was dropped onto the sample immediately, and spinning was continued for 20 s. Finally, the whole film was annealed at 150°C for 15 min.

The precursor was obtained by stirring 1 mL chlorobenzene solution, which contained 72.3 mg Spiro-OMeTAD, 28 μL 4-tert-butylpyridine, and 17 μL Li-TFSI solution (520 mg mL^{-1}). The precursor was spin-coated onto perovskite film at 2000 rpm for 30 s. Then, the Spiro-OMeTAD HTL was obtained.

Characterization Methods

A field-emission scanning electron microscope (FE-SEM, SU8010, Hitachi) was carried out to study the morphologies of the samples. The absorption spectra were recorded with a UV-vis spectrophotometer (Shimadzu, UV-3600). Electrochemical impedance spectroscopy (EIS) was employed to understand the carrier transportation process by an electrochemical workstation (Autolab, PGSTAT 302N). The current density–voltage (J - V) measurement was recorded using a digital source (Keithley 2400) with the assistance of the solar simulator (ABET Technologies, SUN 3000).

Results And Discussion

A schematic of the PSC structure and the Nb: TiO_2 synthesis procedure is shown in Fig. 1. First, the cleaned FTO substrates were placed in the bottom of the petri dish. Second, 1 mL NbCl_5 ethanol solution and 49 mL TiCl_4 aqueous solution were poured on the dish sequentially. Third, the dish was transferred into a oven for hydrothermal reacting at 70°C for 1 h. Finally, the Nb- TiO_2 layer with nano-pin morphology was formed on the FTO substrates. For the preparation of control TiO_2 layer, only TiCl_4 aqueous solution (without NbCl_5 ethanol solution) was dropped into the dish containing FTO substrates.

To understand the effect of Nb doping on the evolution of the TiO_2 layer, the morphologies of the control TiO_2 and Nb-doped TiO_2 were investigated using scanning electron microscopy (SEM) which is shown in Fig. 2. The bare TiO_2 exhibits a much smoother surface, which is a typical morphology of compact TiO_2 layers in planar PSCs. However, 2% of Nb-doped TiO_2 shows a nano-pin texture distributed on the compact layer. The length of the nano-pin was determined to be 50 ± 20 nm. This indicates that the Nb: TiO_2 layer contains a compact TiO_2 layer with a nano-pin morphology on the surface, which is regarded as a mesoporous layer. Therefore, this in-situ-formed Nb: TiO_2 compact-mesoporous layer, which was obtained by a one-step process, actually serves as both a scaffold and an ETL in the PSC. The formation of nano-pin morphology resulted from the hydrothermal reacting with the assistance of NbCl_5 ethanol solution.

The XPS spectra of 2% Nb: TiO₂ film is shown in Fig. 3. Fig. 3a shows the intensity at the entire binding energy range of the 2% Nb: TiO₂ layer. It is found that the Nb/Ti ratio of 1.3% is closed to the element ratio of 2% in the precursor mixture. The peaks located at 458 eV and 464 eV correspond to the binding energy of Ti 2p_{3/2} and Ti 2p_{1/2} as shown in Fig.3b. The Gaussian fitted lines of Nb⁵⁺ can be deconvoluted into two individual peaks which are associated with Nb 3d_{5/2} and Nb 3d_{3/2} at the binding energy of 207 eV and 209 eV (Fig. 3c). The XPS spectra demonstrates the successful doping of Nb in the TiO₂ film.

Fig. 4a shows the absorption spectra of FTO, bare TiO₂/FTO, and Nb-doped TiO₂/FTO. Both bare TiO₂ and Nb-doped TiO₂ exhibit the main absorption edge in the wavelength range of 300-350 nm. The absorption curve of Nb-doped TiO₂ almost overlaps that of bare TiO₂. The energy band gap (E_g) can be calculated based on the absorption spectra using the Tauc equation, which is shown in Fig. 4b. The E_g is 4.55 eV for FTO and 3.5 eV for both bare TiO₂ and Nb doped TiO₂. Therefore, it can be concluded that Nb doping has little influence on the absorption of TiO₂. The light permeation is also not changed during the Nb doping as shown in Fig. S1.

Fig. S2 presents the SEM images of CH₃NH₃PbI₃ perovskite films spin-coated on the bare TiO₂ and Nb-doped TiO₂ films. Thanks to our previously developed non-substrate-selective dynamic two-step spin coating strategy [36], the perovskite films exhibit fewer pinholes and full surface coverage, suggesting that the dynamic spin-coating procedure allows for better control of the film uniformity and coverage. Besides, the average crystalline grain sizes of the perovskite films are very similar. Fig. S3 presents the absorption spectra of the perovskite films deposited on the bare TiO₂ and Nb-doped TiO₂ films. No obvious difference in absorption peak is observed between the perovskite films. These results suggest that the nano-pin morphology formation on the Nb-doped TiO₂ compact-mesoporous layer could have little effect on the perovskite crystallization by dynamic two-step spin coating strategy.

To understand the carrier transportation crossing the ETL/perovskite interfaces, the electrical impedance spectroscopy (EIS) was employed. PSCs were fabricated with the structure of FTO/TiO₂/perovskite film/Spiro-OMeTAD/Au. Fig. 5 shows the Nyquist plots of PSCs based on bare TiO₂ and 2% Nb: TiO₂ layers, and the corresponding equivalent circuit model is shown in the inset. The parameters of EIS were listed in Supplementary Table S1. It is known that the EIS contains two circular arcs [37]. The high-frequency component is attributed to the charge transport resistance (R_{ct}), and the low-frequency component is mainly related to the recombination resistance (R_{rec}) [38]. In the present work, the perovskite/HTL interface is identical for both PSCs, and the only variable affecting R_{ct} and R_{rec} is the perovskite/ETL interface. Compared to the bare TiO₂ device, the Nb: TiO₂ device exhibits smaller R_{ct} and larger R_{rec} . The small R_{ct} contributes to more efficient electron extraction, and the large R_{rec} proves lower

charge recombination. These results confirm that the Nb: TiO₂ compact-mesoporous layer is an effective ETL for simultaneously improving charge transportability and reducing the carrier recombination rate.

As shown in Fig. 6, the dependence of the PCE of PSCs on the Nb doping contents was investigated. The detail parameters for PSCs with different Nb doping concentrations varying from 0% to 8% was shown in Table 1. It is found that the doping ratio affects the open circuit voltage (V_{oc}) and fill factor (FF), which were first increased and then decreased with increasing Nb doping. The device with a 2% Nb-doped TiO₂ layer exhibits the highest V_{oc} of 1.19 eV, J_{sc} of 23.52 mA/cm², and FF of 70.74%, leading to a PCE as high as 19.74% for the champion devices. Thanks to better carrier transportation, all parameters show notable improvement. However, superfluous doping would strengthen the carrier scattering and lead to poor mobility. The incremental recombination will weaken the carrier transport improvement and eventually harm the PCE.

Table 1 Performance parameters of PSCs based on different Nb doping concentrations

Solar cells	V_{oc} (V)	J_{sc} (mA cm ⁻²)	FF (%)	PCE (%)
0% Nb	1.04	23.80	63.56	15.70
2% Nb	1.19	23.52	70.74	19.74
4% Nb	1.17	23.58	70.28	19.31
6% Nb	1.12	23.36	68.88	18.17
8% Nb	1.11	22.93	59.94	15.21

The measured J - V curves of the control and champion device are shown in Fig. 7. It is well known that J - V hysteresis behavior often occurs, especially in planar structure PSC devices. In this work, the hysteresis of J - V curves of bare compact TiO₂-based PSC and 2% Nb:TiO₂ compact-mesoporous layer-based PSC were examined. The hysteresis index, (PCE of reverse scan - PCE of forward scan)/PCE of reverse scan^[30], reduced markedly from 24.39% for the PSC based on bare compact TiO₂ to 3.19% for the PSC based on 2% Nb-doped TiO₂ layer. It is well known that PSCs based on a mesoporous TiO₂ layer can collect electrons and effectively achieve balance between the hole flux and electron flux due to its larger surface area, thereby exhibiting less hysteresis^[17]. The suppression of hysteresis of the J - V curve for the Nb-doped TiO₂ device resulted from the existence of the conductance increasing nano-pin morphology on the surface that is likely to be a mesoporous TiO₂ layer. Charge accumulation caused by interfacial capacitance at the ETL/perovskite interface would be reduced and result in hysteresis-less character.

Conclusion

We have developed a facile one-step, in situ and low-temperature approach to achieve an Nb: TiO₂ compact-mesoporous layer that serves as both scaffold and ETL in PSCs. As a result, a PSC device based on 2% Nb-doped TiO₂ exhibits a maximum PCE of 19.74%, which is dramatically higher than that of the control device based on the bare TiO₂. The Nb:TiO₂ layer contains a compact TiO₂ layer with nanopin morphology on the surface, which is utilized as a mesoporous layer. Due to the collaborative effect of a large interface surface area and improved carrier transportation rate, the hysteresis of the *J-V* curve is markedly reduced, with the hysteresis index decreasing significantly from 24.39% to 3.19%. This work promises an effective approach for achieving hysteresis-less and high-efficiency PSCs through scalable and inexpensive methods at low temperature.

Abbreviations

PSCs: Perovskite solar cells; PCE: Power conversion efficiency; TiO₂: Titanium oxide; ETL: Electron transport layer; SEM: Scanning electron microscope; EIS: Electrochemical impedance spectroscopy; B_g: Band gap; E_g: Energy band gap; *V*_{oc}: Open circuit voltage; FF: Fill factor; *J*_{sc}: Short circuit current density.

Declarations

Acknowledgements

I would like to express my gratitude to the financial support from the National Natural Science Foundation of China (51972042), and the Fundamental Research Funds for the Central Universities (Y0301902300100112).

Authors' Contributions

YM prepared the materials and fabricated the devices. SH and HX carried out XPS, EIS, SEM measurements. YY and ZW wrote the manuscript. All authors read and approved the final manuscript.

Funding

This research was supported by the National Natural Science Foundation of China (51972042), and the Fundamental Research Funds for the Central Universities (Y0301902300100112).

Availability of Data and Materials

The authors declare that the materials and data are available to the readers, and all conclusions made in this manuscript are based on the data which are all presented and shown in this paper.

Competing Interests

The authors declare that they have no competing interests.

References

- 1 Yang M, Li Z, Reese M, et al (2017) Perovskite ink with wide processing window for scalable high-efficiency solar cells. *Nat Energy* 2(5): 17038-17047.
- 2 Zhao D, Chen C, Wang C, et al (2018) Efficient two-terminal all-perovskite tandem solar cells enabled by high-quality low-bandgap absorber layers. *Nat Energy* 3(12): 1093-1100.
- 3 Shi D, Adinolfi V, Comin R, et al (2015) Low trap-state density and long carrier diffusion in organolead trihalide perovskite single crystals. *Science* 347(6221): 519-522.
- 4 Sun H, Lei T, Tian W, et al (2017) Self-powered, flexible, and solution-processable perovskite photodetector based on low-cost carbon cloth. *Small* 13(28): 1701042-1701049.
- 5 Sun H, Tian W, Cao F, et al (2018) Ultrahigh-performance self-powered flexible double-twisted fibrous broadband perovskite photodetector. *Adv Mater* 30(21): 1706986-1706993.
- 6 Zhao Y, Li C, Shen L (2019) Recent advances on organic-inorganic hybrid perovskite photodetectors with fast response. *InfoMat* 1(2): 164-182.
- 7 Zhao X, Xu H, Wang Z, et al (2019) Memristors with organic-inorganic halide perovskites. *InfoMat* 1(2): 183-210.
- 8 Fang T, Zhang F, Yuan S, et al (2019) Recent advances and prospects toward blue perovskite materials and light-emitting diodes. *InfoMat* 1(2): 211-233.
- 9 National renewable energy laboratory, Best research-cell efficiency chart, <https://www.nrel.gov/pv/cell-efficiency.html> (accessed: August 2019)
- 10 Zhang F, Zhu K (2019) Additive engineering for efficient and stable perovskite solar cells. *Adv Energy Mater* 10(13):1902579-19025605.
- 11 Lu P, Lu M, Wang H, et al (2019) Metal halide perovskite nanocrystals and their applications in optoelectronic devices. *InfoMat* 1(4): 430-459.

- 12 Luo J, Xia J, Yang H, et al (2020) Novel approach toward hole-transporting layer doped by hydrophobic Lewis acid through infiltrated diffusion doping for perovskite solar cells. *Nano Energy* 70: 104509-104519.
- 13 Lee M, Teuscher J, Miyasaka T, et al (2012) Efficient hybrid solar cells based on meso-superstructured organometal halide perovskites. *Science* 338(6107): 643-647.
- 14 Fakharuddin A, Schmidt-Mende L, Garcia-Belmonte G, et al (2017) Interfaces in perovskite solar cells. *Adv Energy Mater* 7(22): 1700623.
- 15 Sun H, Zhou Y, Xin Y, et al (2019) Composition and Energy Band-Modified Commercial FTO Substrate for In Situ Formed Highly Efficient Electron Transport Layer in Planar Perovskite Solar Cells. *Adv Funct Mater* 29(11): 1808667-1808676.
- 16 Yang D, Yang R, Wang K, et al (2018) High efficiency planar-type perovskite solar cells with negligible hysteresis using EDTA-complexed SnO₂. *Nat Commun* 9(1): 1-11.
- 17 Yang W, Park B, Jung E, et al (2017) Iodide management in formamidinium-lead-halide-based perovskite layers for efficient solar cells. *Science* 356(6345): 1376-1379.
- 18 Ravishankar S, Gharibzadeh S, Roldán-Carmona C, et al (2018) Influence of charge transport layers on open-circuit voltage and hysteresis in perovskite solar cells. *Joule* 2(4): 788-798.
- 19 Hao D, Zou J, Huang J (2020) Recent developments in flexible photodetectors based on metal halide perovskite. *InfoMat* 2(1): 139-169.
- 20 Yella A, Heiniger L, Gao P, et al (2014) Nanocrystalline rutile electron extraction layer enables low-temperature solution processed perovskite photovoltaics with 13.7% efficiency. *Nano Lett* 14 (5): 2591-2596.
- 21 Mabrouk S, Bahrami B, Elbohy H, et al (2019) Synergistic engineering of hole transport materials in perovskite solar cells. *InfoMat* DOI: 10.1002/inf2.12062.
- 22 Cai F, Yang L, Yan Y, et al (2017) Eliminated hysteresis and stabilized power output over 20% in planar heterojunction perovskite solar cells by compositional and surface modifications to the low-temperature-processed TiO₂ layer. *J Mater Chem A* 5(19): 9402-9411.
- 23 Ren X, Liu Y, Lee D, et al (2020) Chlorine-modified SnO₂ electron transport layer for high-efficiency perovskite solar cells. *InfoMat* 2(2): 401-408.
- 24 Jiang J, Jin Z, Lei J, et al (2017) ITIC surface modification to achieve synergistic electron transport layer enhancement for planar-type perovskite solar cells with efficiency exceeding 20%. *J Mater Chem A* 5: 9514-9522.

- 25 Giordano F, Abate A, Correa B, et al (2016) Enhanced electronic properties in mesoporous TiO₂ via lithium doping for high-efficiency perovskite solar cells. *Nat Commun* 7: 10379-10385.
- 26 Liu D, Li S, Zhang P, et al (2017) Efficient planar heterojunction perovskite solar cells with Li-doped compact TiO₂ layer. *Nano Energy* 31: 462-468.
- 27 Yin G, Ma J, Jiang H, et al (2017) Enhancing efficiency and stability of perovskite solar cells through Nb-doping of TiO₂ at low temperature. *ACS Appl Mater Interfaces* 9(12): 10752-10758.
- 28 Chen B, Rao H, Li W, et al (2016) Achieving high-performance planar perovskite solar cell with Nb-doped TiO₂ compact layer by enhanced electron injection and efficient charge extraction. *J Mater Chem A* 4(15): 5647-5653.
- 29 Jiang L, Wang Z, Li M, et al (2018) Enhanced electrical property of compact TiO₂ layer via platinum doping for high-performance perovskite solar cells. *Sol RRL* 2(11): 1800149-1800157.
- 30 Hou Y, Scheiner S, Tang X, et al (2017) Suppression of hysteresis effects in organohalide perovskite solar cells. *Adv Mater Interfaces* 4(11): 1700007-1700016.
- 31 Roose B, Godel K, Pathak S, et al (2016) Enhanced efficiency and stability of perovskite solar cells through Nd-doping of mesostructured TiO₂. *Adv Energy Mater* 6(2): 1501868-1501875.
- 32 Pathak S, Abate A, Ruckdeschel P, et al (2014) Performance and stability enhancement of dye-sensitized and perovskite solar cells by Al doping of TiO₂. *Adv Funct Mater* 24(38): 6046-6055.
- 33 Liang C, Li P, Zhang Y, et al (2017) Mild solution-processed metal-doped TiO₂ compact layers for hysteresis-less and performance-enhanced perovskite solar cells. *J Power Sources* 372: 235-244.
- 34 Song J, Li S, Zhao Y, et al (2017) Performance enhancement of perovskite solar cells by doping TiO₂ blocking layer with group VB elements. *J Alloys Compd* 694: 1232-1238.
- 35 Kang D, Park N (2019) On the current-voltage hysteresis in perovskite solar cells: dependence on perovskite composition and methods to remove hysteresis. *Adv Mater* 31(34): 1805214.
- 36 Sun H, Deng K, Zhu Y, et al (2018) A novel conductive mesoporous layer with a dynamic two-step deposition strategy boosts efficiency of perovskite solar cells to 20%. *Adv Mater* 30(28): 1801935-1801943.
- 37 Zhang Z, Li J, Wang X, et al (2017) Enhancement of perovskite solar cells efficiency using N-Doped TiO₂ nanorod arrays as electron transfer layer. *Nanoscale Res Lett* 12(1): 43-50.
- 38 Liu D, Yang J, Kelly T (2014) Compact layer free perovskite solar cells with 13.5% efficiency. *J Am Chem Soc* 136(49): 17116-17122.

Figures

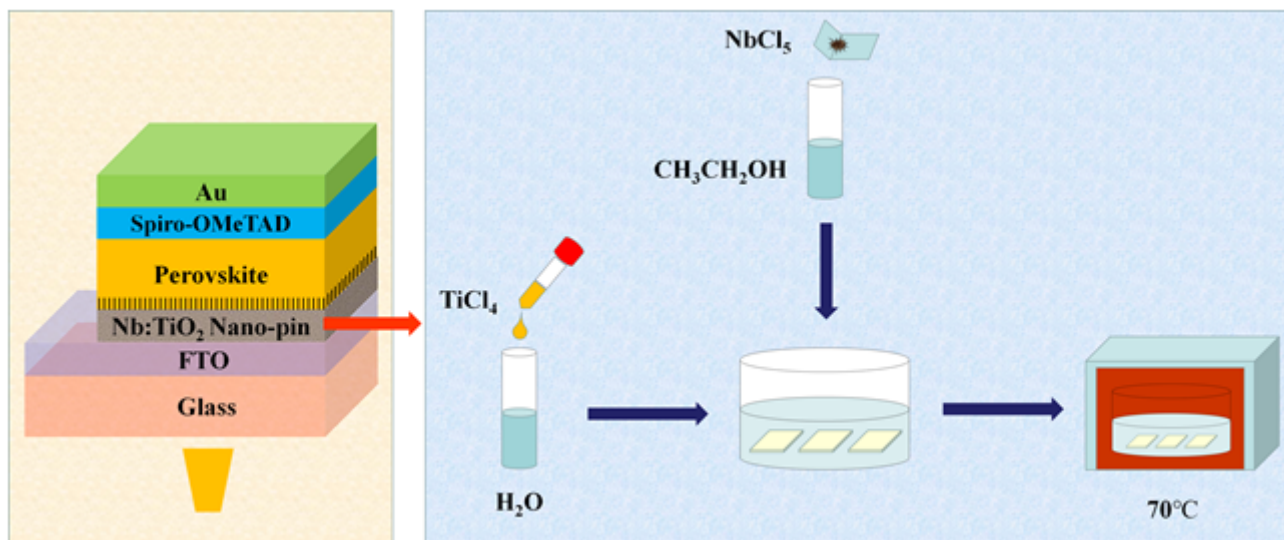


Figure 1

Schematic of PSC structure and Nb: TiO₂ synthesis procedure.

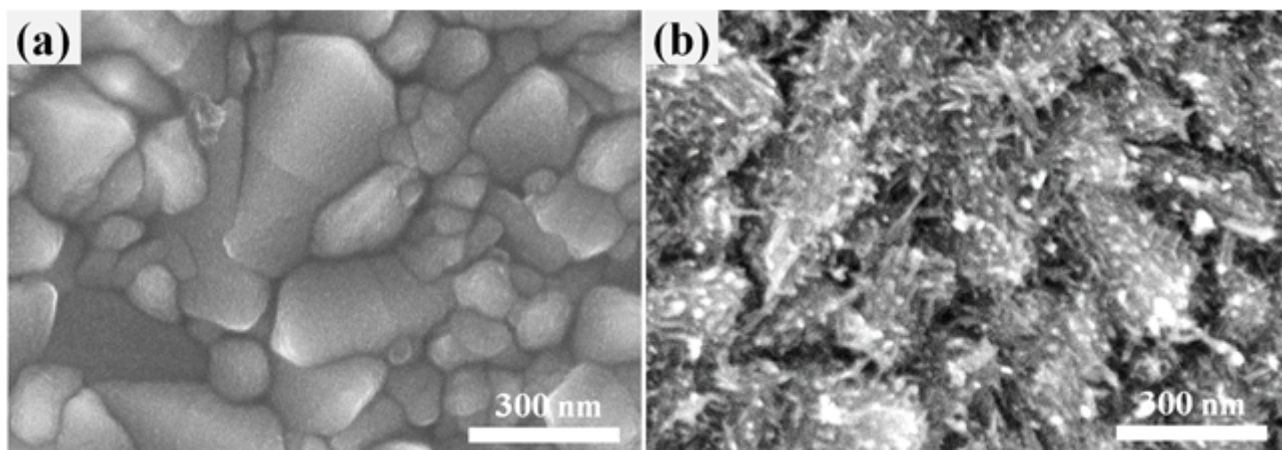


Figure 2

Top-view SEM images of (a) TiO₂/FTO, and (b) 2% Nb: TiO₂/FTO.

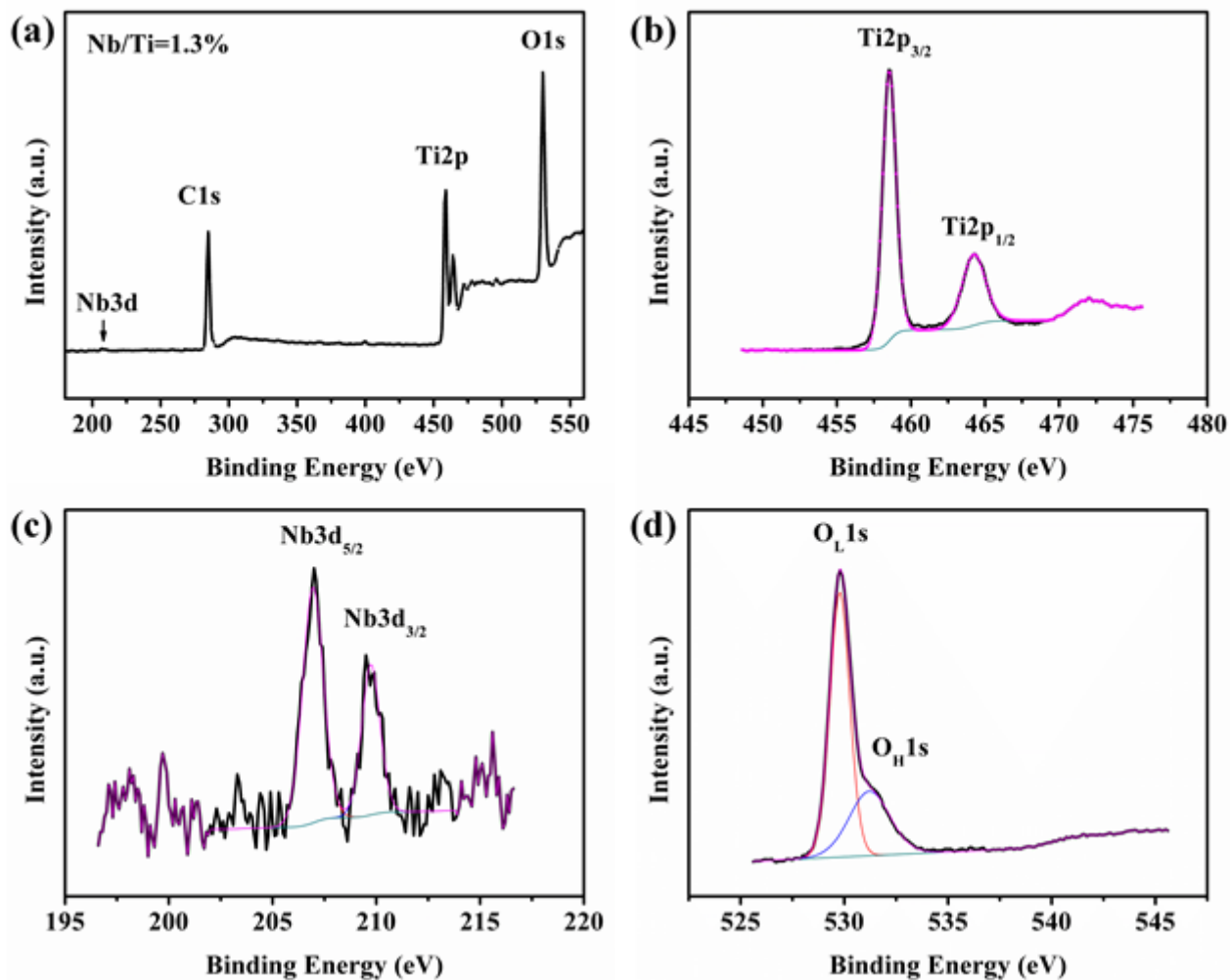


Figure 3

XPS spectra of 2% Nb:TiO₂. (a) Survey, (b) Ti 2p, (c) Nb 3d, and (d) O 1s.

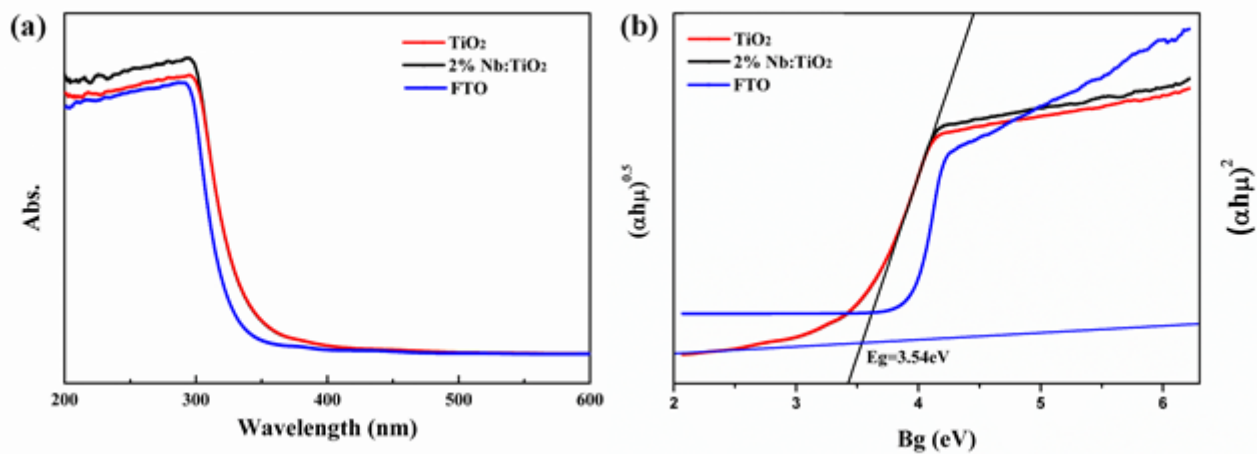


Figure 4

(a) The absorption spectra of the FTO substrate, TiO₂/FTO and 2% Nb:TiO₂ /FTO. (b) Tauc-plots of the FTO substrate, TiO₂/FTO and 2% Nb:TiO₂ /FTO.

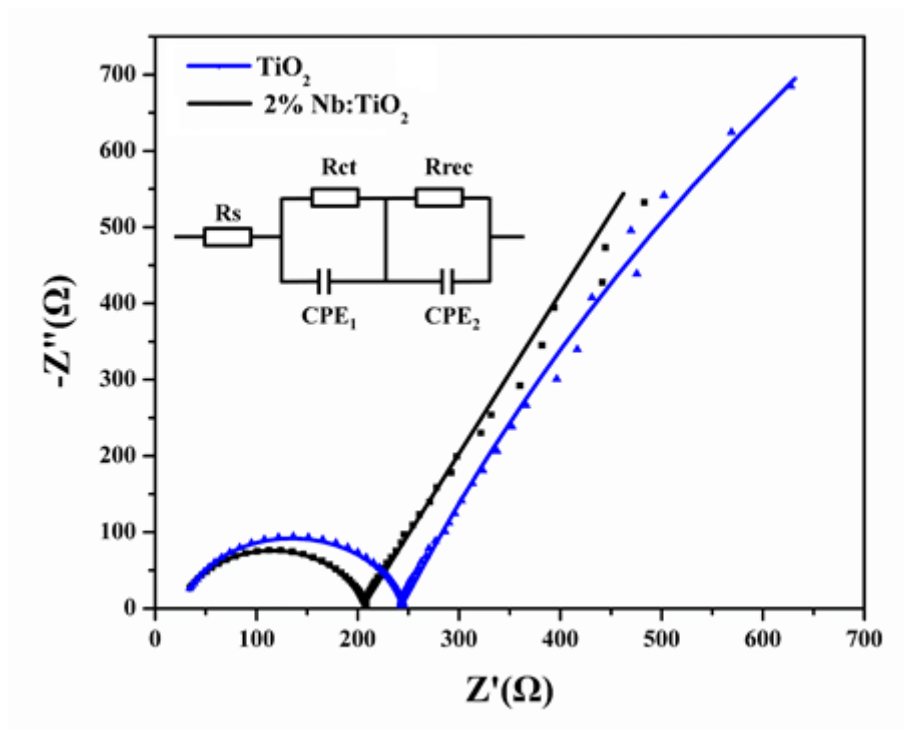


Figure 5

Nyquist plots of devices based on bare TiO₂ and 2% Nb-doped TiO₂ layers.

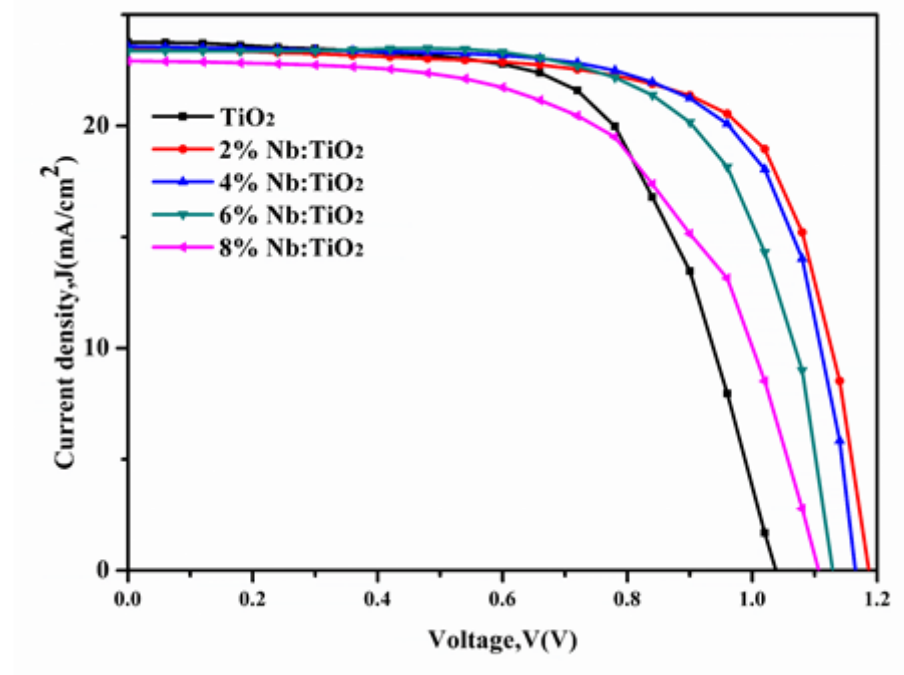


Figure 6

J-V curves of PSCs based on different Nb doping concentrations

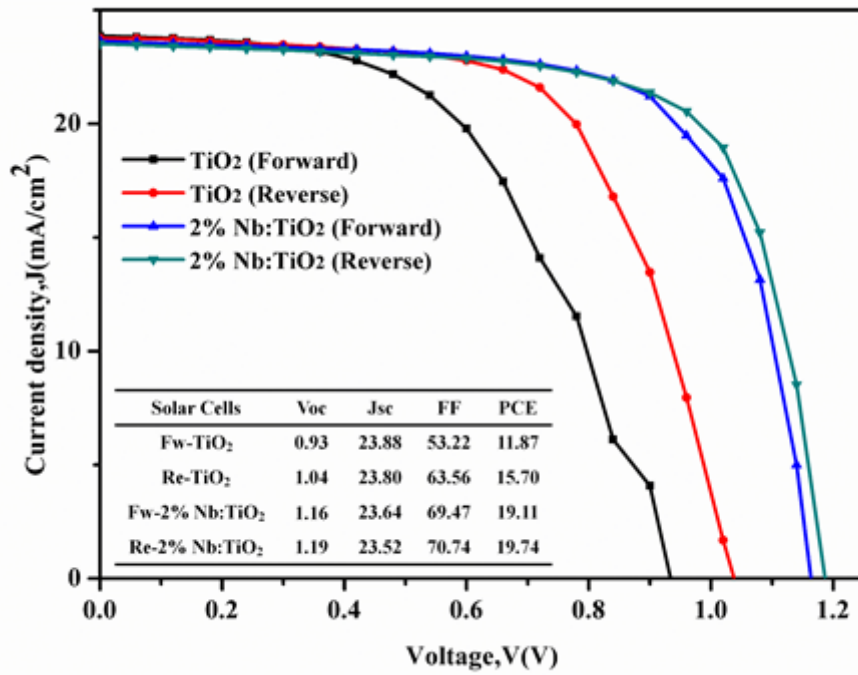


Figure 7

The J-V hysteresis behavior of the PSCs based on bare TiO₂ and 2% Nb: TiO₂ layer under AM 1.5 illumination.

Supplementary Files

This is a list of supplementary files associated with this preprint. Click to download.

- [Fig.S2.tif](#)
- [Fig.S3.tif](#)
- [SInanoscaleresearchletters.docx](#)
- [Fig.S1.tif](#)